Arf-GEF localization and function at myosin-rich adherens junctions via coiled-coil heterodimerization with an adaptor protein

Shiyu Zheng†, Junior J. West†, Cao Guo Yu, and Tony J. C. Harris*
Department of Cell and Systems Biology, University of Toronto, Toronto, ON M5S 3G5, Canada

ABSTRACT **Tissue dynamics require regulated interactions between adherens junctions and cytoskeletal networks. For example, myosin-rich adherens junctions recruit the cytohesin Arf-GEF Steppke, which down-regulates junctional tension and facilitates tissue stretching. We dissected this recruitment mechanism with structure–function and other analyses of Steppke and Stepping stone, an implicated adaptor protein. During *Drosophila* dorsal closure, Steppke's coiled-coil domain was necessary and sufficient for junctional recruitment. Purified coiled-coil domains of Steppke and Stepping stone heterodimerized through a hydrophobic surface of the Steppke domain. This mapped surface was required for Steppke's junctional localization and tissue regulation. Stepping stone colocalized with Steppke at junctions, and was required for junctional Steppke localization and proper tissue stretching. A second conserved region of Stepping stone was necessary and largely sufficient for junctional localization. Remarkably, this region could substitute for the Steppke coiled-coil domain for junction localization and regulation, suggesting the main role of the Steppke coiled-coil domain is linkage to the junctional targeting region of Stepping stone. Thus, coiled-coil heterodimerization with Stepping stone normally recruits Step to junctions. Intriguingly, Stepping stone's junctional localization also seems partly dependent on Steppke.**

Monitoring Editor
Yukiko Yamashita
University of Michigan

Received: Oct 15, 2019
Accepted: Oct 28, 2019

INTRODUCTION

Epithelia provide regulated barriers for organ structure and function. These multicellular sheets also undergo amazing dynamics. Epithelial cells can change shape and interactions while assembling, disassembling, and remodeling the adherens junctions (AJs) that connect them. The classical cadherins of AJs (such as *Drosophila* E-cadherin [DE-cad]) mediate homophilic cell–cell adhesion and link to cortical actin networks through the adaptor proteins β-catenin and α-catenin (Harris and Tepass, 2010; Takeichi, 2014). These cadherin–catenin complexes also transduce signals for AJ growth and regulation. Such signaling can be biochemical, such as the local induction of Arp2/3-based actin networks for junction growth (Ratheesh *et al.*, 2013), or the regulated recruitment of endocytic machinery for junction removal (Cadwell *et al.*, 2016). Additionally, mechanical signal transduction occurs. For example, actomyosin-based tension can unfurl α-catenin to expose binding sites for proteins such as Vinculin, which then reinforce AJ–actin interactions (Leckband and de Rooij, 2014; Pinheiro and Bellaïche, 2018; Yap *et al.*, 2018). AJ regulatory signaling is an area of intense research, and many mechanisms remain incompletely understood.

Actomyosin activity at AJs has been shown to recruit the cytohesin Arf-GEF Steppke (Step) during *Drosophila* dorsal closure (West *et al.*, 2017) and in *Drosophila* wing discs (Rauskolb *et al.*, 2019). This recruitment is part of a negative feedback loop that antagonizes junctional actomyosin contractility through Step Arf-GEF activity. During dorsal closure, the negative feedback allows orderly stretching of the epidermis. Without Step, heightened junctional actomyosin activity holds local cell groups in distorted configurations (multicellular rosettes). Cytohesin Arf-GEFs also down-regulate actomyosin for zebrafish epiboly (West *et al.*, 2017), for the partial cleavage of the syncytial *Drosophila* embryo (Lee and Harris, 2013), for proper organization of the Drosophila wing disc epithelium

This article was published online ahead of print in MBoC in Press (http://www.molbiolcell.org/cgi/doi/10.1091/mbc.E19-10-0566) on November 6, 2019.

†These authors contributed equally to this work.

*Address correspondence to: Tony J. C. Harris (tony.harris@utoronto.ca). ORCID: 0000-0002-0798-970X.

Abbreviations used: AJs, adherens junctions; A–P, anterior–posterior; CC, coiled-coil; CR, conserved region; DE-cad, *Drosophila* E-cadherin; LE, leading edge; PH, pleckstrin homology; Sstn, Stepping stone; Step, Steppke.

(Rauskolb *et al.*, 2019), and for mammalian cell podosome formation (Rafiq *et al.*, 2017).

Cytohesins contain a central Sec7 domain that conveys Arf-GEF activity, as well as two domains implicated in plasma membrane recruitment: an N-terminal coiled-coil (CC) domain and a C-terminal pleckstrin homology (PH) domain (Gillingham and Munro, 2007; Donaldson and Jackson, 2011). Cytohesin PH domains bind either PIP2 or PIP3 (Klarlund *et al.*, 2000)—the Step PH domain preferentially binds PIP3 (Britton *et al.*, 2002; Lee *et al.*, 2015)—and separate sites of the PH domain can also bind Arf6 and Arl4 (Cohen *et al.*, 2007; Hofmann *et al.*, 2007). The CC domains of cytohesins can bind to a variety of adaptor proteins, including CNK1, GRASP/Tamalin, FRMD4A, and GRSP-1 (Nevrivy *et al.*, 2000; Ikenouchi and Umeda, 2010; Lim *et al.*, 2010; Hahn *et al.*, 2013). Relevant to AJs, FRMD4A and GRSP-1 both bind cytohesin-1 via CC domain heterodimerization and to the AJ-associated protein Par-3 through a separate site, and these interactions recruit cytohesin-1 to nascent AJs for their maturation in mammalian cell culture (Ikenouchi and Umeda, 2010). Of note, cytohesin CC domains can also undergo homodimerization (DiNitto *et al.*, 2007; Liu *et al.*, 2015), and have additionally been implicated in cytohesin autoinhibition through interaction with the PH domain (Li *et al.*, 2012; Hiester and Santy, 2013).

From cleavage-stage *Drosophila* embryos, Stepping stone (Sstn) was identified as the main protein to coimmunoprecipitate with Step (Liu *et al.*, 2015). The closest mammalian homologue of Sstn was found to be FRMD4A. In vitro, Sstn and Step were shown to bind directly, and this interaction required each protein's CC domain. In vivo, embryos depleted of Sstn or Step displayed similar cleavage-stage actomyosin misregulation defects, and overexpressed versions of the proteins displayed striking colocalization at myosin-rich domains of pseudocleavage furrows. Step localization to these domains required its CC domain, whereas the Sstn localization required a separate region of the protein conserved in insects (termed conserved region [CR]; Liu *et al.*, 2015). Liu *et al.* (2015) studied the syncytial embryo before cells and AJs had formed. More recently, overexpressed versions of Step and Sstn were also found to colocalize at AJs of *Drosophila* wing discs, and the AJ localization of overexpressed Step was diminished by depletion of Sstn (Rauskolb *et al.*, 2019). Moreover, depletions of Step or Sstn resulted in excessive junctional actomyosin in the wing disc (Rauskolb *et al.*, 2019). The studies of Liu *et al.* (2015) and Rauskolb *et al.* (2019) suggest a model of how Step–Sstn interaction could mediate Step recruitment to myosin-rich AJs. We sought to test this model by addressing the following questions. Step and Sstn are recruited to both myosin-rich domains of pseudocleavage furrows and to myosin-rich AJs, but do their protein domains play similar roles in both contexts? The CC domain of Step is required for direct binding to Sstn in vitro and for Step localization to pseudocleavage furrows, but is heterodimerization with Sstn the major role of the Step CC domain in vivo? A requirement of Sstn for the AJ localization of Step is evident, but is the relationship just unidirectional? Also, what are the relationships between endogenously expressed Step and Sstn?

Dorsal closure of the *Drosophila* embryo is an excellent model for examining regulation of junctional actomyosin activity during tissue morphogenesis (Kiehart *et al.*, 2017). During this process, lateral epidermal sheets elongate dorsally to cover the amnioserosa, a dorsal, extraembryonic tissue. Contraction of the aminoserosa plays a major role in pulling the lateral epidermis dorsally, and the epidermis reorganizes as it stretches through the growth of cell–cell contacts at the anterior and posterior of each cell (A–P contacts). Myosin and Step normally display enrichments at tricellular junctions throughout the epidermis (Young *et al.*, 1993; West *et al.*, 2017), and Step Arf-GEF activity at these sites seems to antagonize junctional actomyosin to eliminate multicellular rosettes from the rectangular array of elongating cells (West *et al.*, 2017). Myosin enrichment at tricellular junctions is also evident in the *Drosophila* wing disc (Major and Irvine, 2006; Rauskolb *et al.*, 2019), and in vertebrate tissues (Campinho *et al.*, 2013; Reyes *et al.*, 2014; West *et al.*, 2017). In addition, a robust, tension-bearing, supracellular actomyosin cable forms along the epidermal leading edge (LE) to coordinate its forward movement (Kiehart *et al.*, 2017). Because the LE is multicellular, the cable is composed of many actomyosin bundles connected by AJs. The individual actomyosin bundles of the supracellular cable are remarkably uniform in length, and these lengths are controlled by Step and other regulators of junctional actomyosin, such as Ajuba and Canoe (*Drosophila* Afadin), which are all enriched at LE junctions (West *et al.*, 2017; Manning *et al.*, 2019; Rauskolb *et al.*, 2019).

We report structure–function analyses, in vitro binding assays, colocalization tests, and mutant studies that identify a mechanism of Step recruitment to myosin-rich AJs. The Step CC domain was found to be both necessary and sufficient for the recruitment. Direct Step-Sstn CC domain heterodimerization was detected in vitro, and an interaction interface was mapped and shown to be required for Step localization and function at dorsal closure. Our data revealed close colocalization of endogenously expressed Step and Sstn at myosin-rich junctions. Endogenous Step required Sstn for its junctional localization, and intriguingly, the junctional localization of endogenous Sstn also relied substantially on Step. Thus, Step and Sstn may support each other's localization as an interacting pair. Additionally, the Sstn CR was found to be necessary and largely sufficient for localization to myosin-rich junctions, and could functionally substitute for the Step CC domain, implicating Sstn function as an adaptor between Step and junctions.

RESULTS

The CC domain of Step is necessary and sufficient for LE and tricellular junction localization

To investigate how deletion of the CC domain or the PH domain of Step affects the recruitment of Step to AJs at dorsal closure, we compared three previously generated constructs: GFP-tagged full-length Step, StepΔCC, and StepΔPH (Figure 1A shows all Step and Sstn constructs used for the in vivo structure–function analyses of this article; Lee and Harris, 2013; Lee *et al.*, 2015; Liu *et al.*, 2015). Expression of the UAS constructs was driven with *daughterless*-Gal4 from the same genomic site (the constructs were each inserted at the attp40 recombination site on chromosome 2 to avoid positional effects on transcription) and imaged live during dorsal closure with the same microscope settings (to allow comparisons of signal intensities between constructs). Full-length Step was enriched most strongly at epidermal LE and tricellular junctions (Figure 1B; white arrow indicates the LE and yellow arrows indicate tricellular junctions of the lateral epidermis), and less so at bicellular junctions of the lateral epidermis (Figure 1, B and E; West *et al.*, 2017). GFP-StepΔPH showed a similar localization pattern as full-length GFP-Step, with statistically indistinguishable distributions among the junction types (Figure 1, B and E). In contrast, removal of the CC domain severely perturbed the localization pattern. GFP-StepΔCC displayed a relatively low level of general plasma membrane localization (observed consistently in comparisons of eight embryos expressing full-length GFP-Step and seven embryos expressing GFP-StepΔCC), without substantial enrichment at epidermal LE or tricellular junctions (Figure 1, B and E).

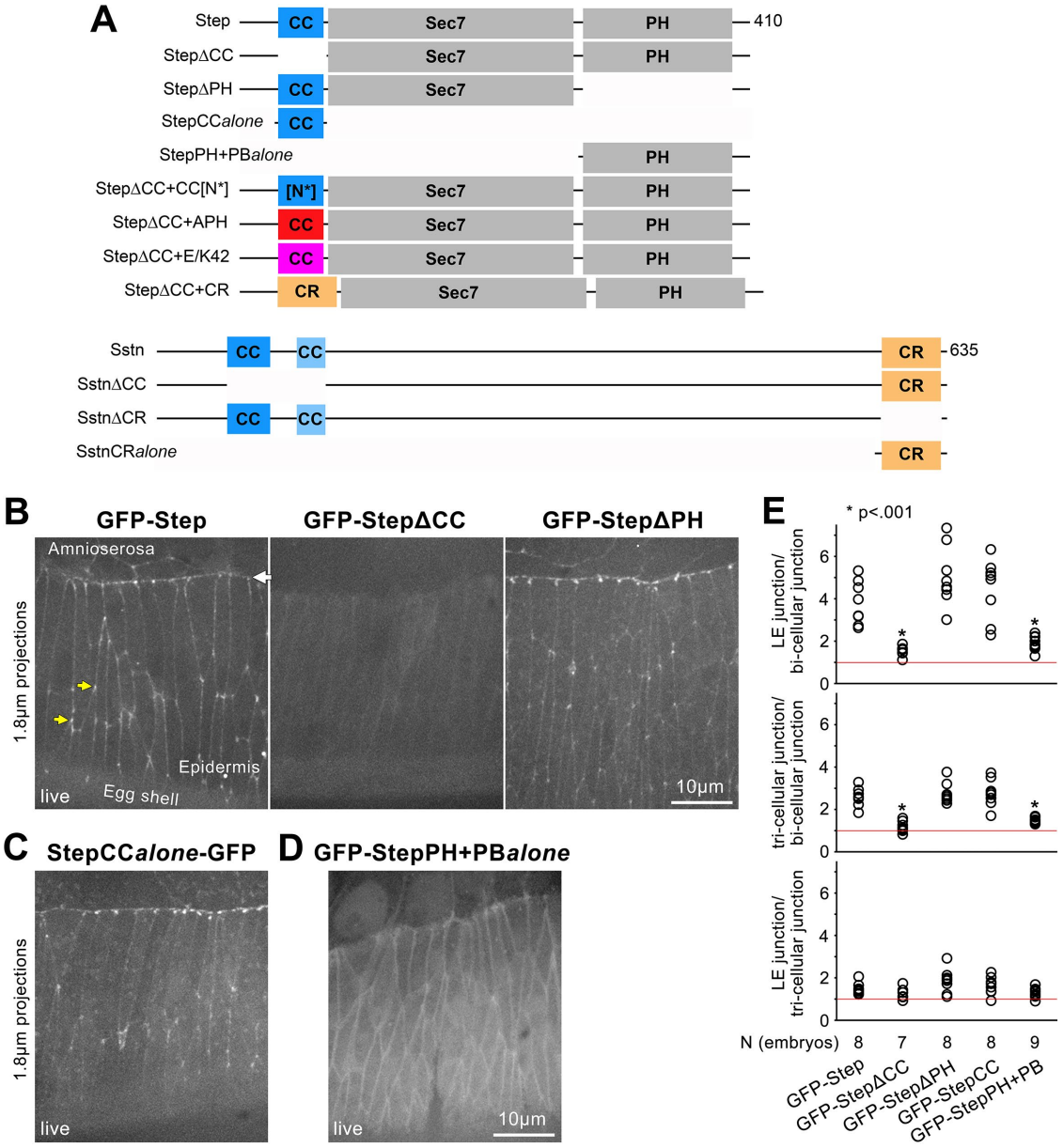

FIGURE 1: The Step CC domain is important for localization to LE and tricellular junctions. (A) Schematics of all Step and Sstn constructs used for the in vivo structure–function analyses of this article. (B, C) Constructs were expressed with the Gal4-UAS system using *daughterless*-Gal4 and images were collected and adjusted with the same settings. (B) Embryos during dorsal closure expressing full-length and domain deletion Step constructs in the lateral epidermis and amnioserosa (the top portion of each image). White arrow indicates the LE and yellow arrows indicate tricellular junctions of the lateral epidermis. Both GFP-Step and GFP-StepΔPH are enriched at epidermal LE and tricellular junctions. GFP-StepΔCC shows a disperse plasma membrane localization. (C) A dorsal closure embryo with enrichment of StepCC*alone*-GFP to epidermal LE and tricellular junctions. (D) A dorsal closure embryo with disperse localization of GFP-StepPH+PB*alone* over the plasma membrane. This construct was expressed with a distinct system (see *Materials and Methods*) and was imaged with distinct settings. (E) Signal intensity ratios between junctions of interest: "LE junction" refers to junctions of the epidermal LE; "tricellular junction" refers to tricellular junctions of epidermal cells to the rear; and "bicellular junction" refers to A–P bicellular junctions of epidermal cells to the rear. Asterisks indicate significant differences from full-length GFP-Step. Red lines indicate ratios of 1:1.

Deletion of the CC domain could affect the location of Step because a specific interaction site was eliminated or because overall Step structure was destabilized. Thus, we tested whether the Step CC domain alone was sufficient for conveying the full-length Step localization pattern. UAS-StepCC*alone*-GFP was generated and expressed using *daughterless*-Gal4. Remarkably, StepCC*alone*-GFP was enriched at epidermal LE and tricellular junctions in a pattern resembling that of full-length GFP-Step (Figure 1, C and E). To test the localization capability of the Step PH domain, we imaged a GFP-tagged construct of the Step PH domain together with its C-terminal polybasic region constitutively driven by a tubulin promoter, a construct called "tGPH," which was developed as a PIP3 marker in

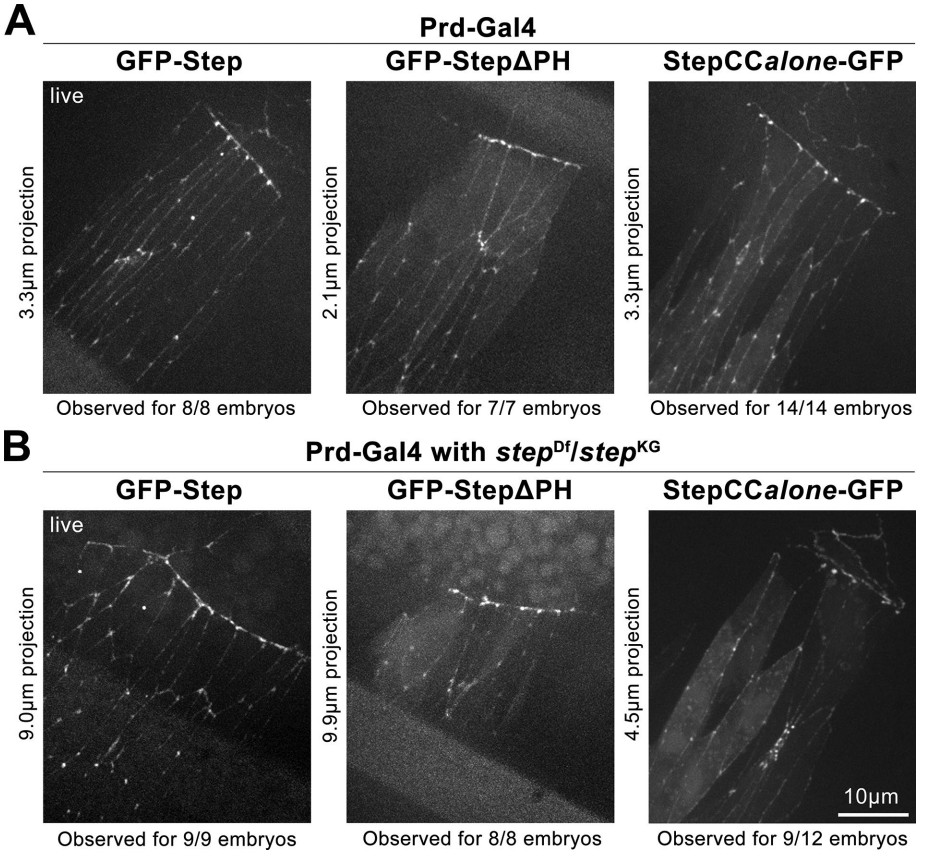

FIGURE 2: Endogenous Step has no apparent effect on the localization of Step constructs containing the CC domain. (A) Live detection of indicated constructs expressed with *paired*-Gal4 in a wild-type background. (B) Live detection of indicated constructs expressed with *paired*-Gal4 in a *step* mutant background. Each construct was imaged with the same settings in the wild-type and *step* mutant backgrounds. Note the tricellular junction enrichment of all constructs in both contexts. Embryo numbers combined from two experiments are shown at the bottom of each image.

Drosophila (Britton *et al.*, 2002). This construct displayed general plasma membrane localization with marginal enrichment to the LE (Figure 1, D and E).

Overall, these results indicate that the CC domain of Step is necessary and sufficient for its enrichment at myosin-rich AJs, and that the PH domain is neither necessary nor sufficient. Because the Step CC domain, like the CC domains of other cytohesins, can homodimerize (DiNitto *et al.*, 2007; Liu *et al.*, 2015), and GFP-StepΔPH and StepCC*alone*-GFP both contain the CC domain, we investigated whether endogenous Step influences the localization of these constructs by expressing them with *paired*-Gal4 in a *step* zygotic mutant background in which maternal Step levels are undetectable at dorsal closure (West *et al.*, 2017). In this context, GFP-StepΔPH and StepCC*alone*-GFP were both enriched at epidermal LE and tricellular junctions to a similar degree as full-length GFP-Step in both control and *step* mutant backgrounds (Figure 2, A and B). Thus, endogenous Step had no apparent effect on the ability of the Step CC domain to target constructs to myosin-rich AJs.

The CC domains of Step and Sstn directly interact through a hydrophobic face of the Step domain

A direct in vitro interaction between Step and Sstn was previously shown to be abolished by deletion of the CC domain of either purified, full-length protein (Liu *et al.*, 2015). To test for direct interaction between the CC domains themselves, and to pursue residues within the CC domains responsible for binding, we purified wild-type or mutated CC domains.

Coiled coils form from the interactions of CC domains. CC domains consist of an α-helix with a hydrophobic face flanked by polar amino acid residues. Interactions between the hydrophobic residues form the core interface of a coiled coil, and interactions of hydrophobic and polar residues additionally determine the orientation and specificity of the interaction (Mason and Arndt, 2004; Grigoryan and Keating, 2008). Using the Phyre2 web portal, the structure of the CC domain of Step was predicted based on sequence similarities to CC domains with known structures (Kelley *et al.*, 2015). The predicted structure was then analyzed with CN3D software to localize hydrophobic residues (Wang *et al.*, 2000). A hydrophobic face was detected along the full length of the predicted structure of the Step CC domain (Figure 3A).

MBP- and GST-tagged forms of the CC domains of Step and Sstn were generated and used in blot overlay assays to test for direct interaction. GST-StepCC showed strong interaction with MBP-SstnCC and vice versa (Figure 3C, asterisks), but no homodimerization of either protein was detected (Figure 3C). To test whether the hydrophobic residues of the Step CC domain were necessary for this interaction, three mutated constructs were tested: the hydrophobic residues were mutated to polar serine residues along the full length of the CC domain, or only along its N-terminal half or its C-terminal half (Figure 3B shows the wild-type and altered Step CC domains as well as the wild-type Sstn CC domain used in the in vitro binding assays). Strikingly, none of the mutated Step CC domains showed any interaction with the Sstn CC domain (Figure 3D), in contrast with the strong binding of the control wild-type Step CC domain (Figure 3D, asterisk). Thus, the CC domains of Step and Sstn interact directly and this interaction requires the full hydrophobic region of the Step CC domain.

The Step-Sstn interaction site is necessary for Step localization, and Step homodimerization seems irrelevant

To test the role of the Step-Sstn binding site in vivo, we inserted the sequence for StepCC[N*] into GFP-Step to replace the wild-type CC domain with the mutated CC domain (creating GFP-StepΔCC+CC[N*]). Because all three mutated Step CC domains abrogated binding to the Sstn CC domain in vitro, we selected StepCC[N*] for the in vivo analysis because we expected it to have less chance of disrupting full-length Step structure—it contains fewer mutations than StepCC[N*+C*], and compared with StepCC[C*] the StepCC[N*] mutations are farther from the Sec7 and PH domains. GFP-StepΔCC+CC[N*] was expressed in vivo using *daughterless*-Gal4. In contrast to full-length GFP-Step, GFP-StepΔCC+CC[N*] failed to enrich at epidermal LE or tricellular junctions, and instead displayed a more general plasma membrane localization pattern which included enrichment at protrusions of the LE and of epidermal cells to the rear (Figure 4, cyan arrows). We noted that the general

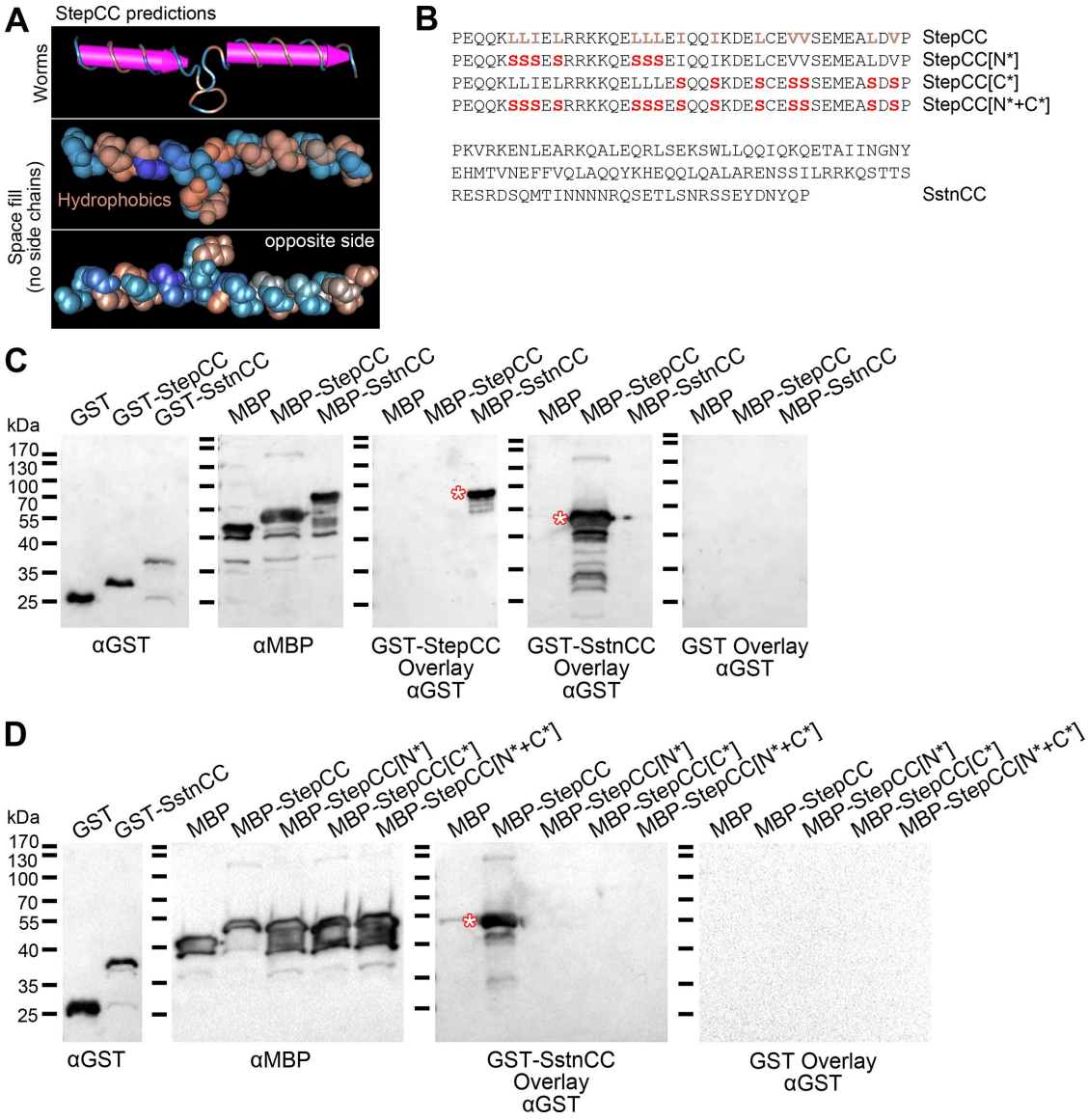

FIGURE 3: The Step and Sstn CC domains bind directly through hydrophobic residues. (A) Step CC domain structure prediction from Phyre2. CN3D viewer images shown. Hydrophobic residues are brown. (B) The Step CC domain sequence is shown at the top. The wild-type domain contains hydrophobic leucine, isoleucine, and valine residues (shown in brown). For StepCC[N*], the first seven hydrophobic residues were changed to polar serine residues (shown in red). For StepCC[C*], the last seven hydrophobic residues were changed to serine residues, and for [N*+C*], all 14 changes were made. The Sstn CC domain sequence is shown at the bottom. (C) Blot overlays of Step CC domain fusion proteins, Sstn CC domain fusion proteins, and control proteins. The αGST and αMBP blots show the relative protein levels used in the overlay experiments with control GST and MBP proteins at equal or higher levels than the CC domain fusion proteins. The αGST blot of the GST-StepCC overlay experiment only shows an interaction between GST-StepCC and MBP-SstnCC (asterisk). The αGST blot of the GST-SstnCC overlay only shows an interaction between GST-SstnCC and MBP-StepCC (asterisk). The αGST blot of the GST control overlay showed no interactions. This overall overlay experiment was replicated separately twice. (D) Blot overlays of wild-type and mutated Step CC domain fusion proteins with the Sstn CC domain fusion proteins. The αGST and αMBP blots show the relative protein levels used in the overlay experiments with control GST and MBP proteins at equal or higher levels than the CC domain fusion proteins. The αGST blot of the GST-SstnCC overlay of the MBP control and wild-type and mutated Step CC domain fusion proteins only showed an interaction between GST-SstnCC and MBP-StepCC (asterisk). The αGST blot of the GST control overlay showed no interactions. These overall overlay results were replicated separately twice.

plasma membrane localization of GFP-StepΔCC+CC[N*] was more easily detected than that of GFP-StepΔCC, suggesting better general stability of GFP-StepΔCC+CC[N*].

To further address the possible influence of Step CC domain homodimerization, we sought to replace the CC domain of Step with a CC domain capable of homodimerization but that would not interact with Sstn. Two CC domains were selected from the literature: APH and E/K42. Both are synthetic sequences optimized for CC homodimerization in vitro. The APH sequence does so in an antiparallel orientation (Gurnon *et al.*, 2003), and the E/K42 sequence does so in a parallel orientation (Graddis *et al.*, 1993). Two constructs were generated to replace the wild-type Step CC domain

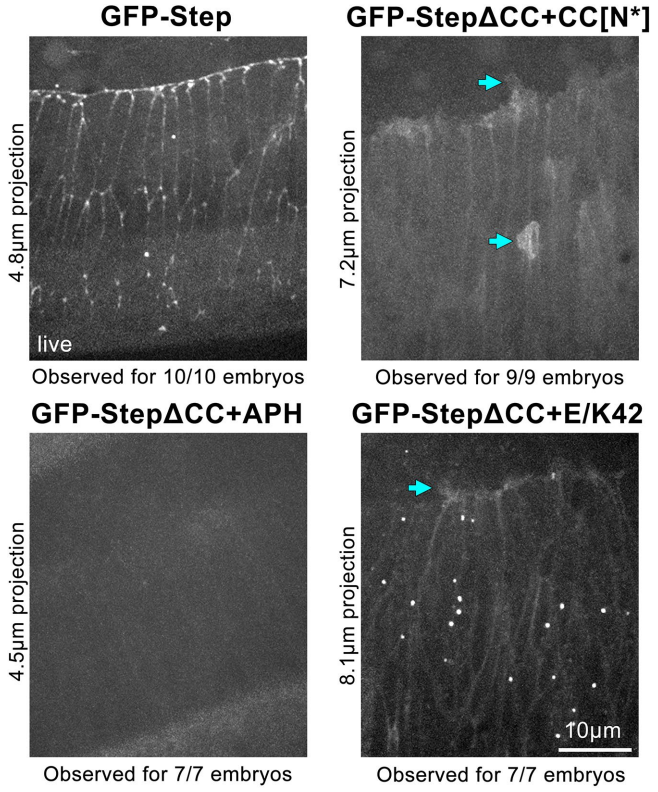

FIGURE 4: Mutating or replacing the CC domain of Step disrupts Step localization. All images were taken live with the same settings at dorsal closure (the amnioserosa is at the top of each image). Construct expression was driven with *daughterless*-Gal-4. Full-length GFP-Step localized to the LE and tricellular junctions of the epidermis. GFP-StepΔCC+CC[N*] displayed a diffuse plasma membrane distribution with some enrichment to cell protrusions at the LE and within the epidermis (cyan arrows). A relatively high cytosolic pool was also apparent. GFP-StepΔCC+APH was very weakly detected and appeared to localize diffusely over the plasma membrane. GFP-StepΔCC+EK42 was detected evenly over the plasma membrane with some enrichment to cell protrusions (cyan arrow). Also, a number of very bright puncta appeared to be cytosolic. Embryo numbers combined from two experiments are shown at the bottom of each image.

with either synthetic CC domain, and the constructs were expressed in vivo using *daughterless*-Gal4. Neither protein displayed the epidermal LE and tricellular junction enrichment of full-length GFP-Step. GFP-StepΔCC+APH was weakly expressed (Figure 4). GFP-StepΔCC+EK42 was more strongly expressed but localized generally to the plasma membrane with enrichment at LE protrusions (Figure 4, cyan arrow). Taken together, these results suggest the specific importance of CC heterodimerization with Sstn for the junctional localization of overexpressed Step constructs.

The Sstn CR is necessary and sufficient for Sstn localization

Next, we performed a structure–function analysis to investigate how Sstn is localized. As Sstn only has two distinctive regions, the CC domain and the region conserved across insects (Liu *et al.*, 2015), we compared full-length Sstn with SstnΔCC and SstnΔCR, each tagged with GFP and inserted at the same genomic site (Liu *et al.*, 2015), after expression with *daughterless*-Gal4. Full-length GFP-Sstn localized in a similar pattern as Step, with highest enrichment at epidermal LE and tricellular junctions (Figure 5A). GFP-SstnΔCC had similar junctional levels compared with GFP-Sstn (Figure 5A; observed for 6/6 GFP-SstnΔCC embryos compared with 8/8 GFP-Sstn embryos), and its distribution resembled that of GFP-Sstn, except for less accumulation at LE junctions relative to other epidermal junctions (Figure 5, A and B). More strikingly, GFP-SstnΔCR showed a drastic loss of signal compared with full-length GFP-Sstn at all junctions (Figure 5A; observed for 8/8 GFP-SstnΔCR embryos compared with 8/8 GFP-Sstn embryos). Despite this loss, the residual cortical SstnΔCR did show some, although reduced, enrichment at epidermal LE and tricellular junctions (Figure 5B).

Because loss of the CR might destabilize Sstn, we tested whether the CR is sufficient for mediating junctional localization. The Sstn CR was tagged with GFP, driven by *daughterless* Gal4, and imaged live at dorsal closure. Strikingly, the Sstn CR was sufficient for enrichment to epidermal LE and tricellular junctions (Figure 5, A and B), although its enrichment to LE junctions was less than that of full-length Sstn (Figure 5, A and B). Thus, the CR of Sstn is necessary and sufficient for mediating much of the localization observed for full-length Sstn. In addition, the CC domain of Sstn contributes to Sstn recruitment to LE junctions.

Replacement of the Step CC domain with the Sstn CR conveys Step localization

Because Step and Sstn were shown to interact via their respective CC domains and the Sstn CR was shown to be sufficient for substantial junctional localization, we hypothesized that the main role of the Step CC domain is to link Step to the Sstn CR through heterodimerization. A prediction from this hypothesis is that the interaction of Step and Sstn could be bypassed by replacing the Step CC domain with the Sstn CR. Thus, we generated a Step construct that substituted the Step CC domain with the Sstn CR, GFP-StepΔCC+CR, and expressed it with *daughterless*-Gal4 for live imaging at dorsal closure. GFP-StepΔCC was imaged in parallel as a negative control, and as discussed, it displayed weak, general plasma membrane localization (Figure 5C). When the Sstn CR replaced the Step CC domain, however, enrichment to epidermal LE and tricellular junctions occurred (Figure 5C; seen for comparisons of 8/8 embryos each). Thus, the Sstn CR can convey substantial localization activity to a Step construct lacking its CC domain.

Step and Sstn colocalize at tricellular junctions

Overexpressed Step and Sstn constructs can colocalize at myosin-rich cortical domains of the syncytial *Drosophila* embryo (Liu *et al.*, 2015), and overexpressed Step and Sstn constructs have each been shown to localize to AJs of *Drosophila* wing discs (Rauskolb *et al.*, 2019). To assess whether the overexpressed proteins colocalize at dorsal closure, *daughterless*-Gal4 was used to coexpress full-length GFP-Step with an mCherry-tagged construct of Sstn (Liu *et al.*, 2015) and both were coimaged live. GFP-Step and mCherry-Sstn displayed close colocalization with both enriched most strongly at epidermal LE and tricellular junctions (Figure 6A). Side views showed the proteins enriched at the apicolateral domain (Figure 6A), where AJs are found.

To assess the localization of Step and Stsn expressed at endogenous levels, we compared proteins expressed from a GFP-tagged *step* allele and from a GFP-tagged *sstn* allele. These alleles were produced by a CRISPR/Cas9 protocol that added the sequence for GFP at the 3′ end of the sequence for each endogenous gene's coding region (see *Materials and Methods*). Indicating normal expression and function of the tagged proteins, each line was homozygous viable and fertile. Live imaging at dorsal closure with the same microscope settings revealed strong

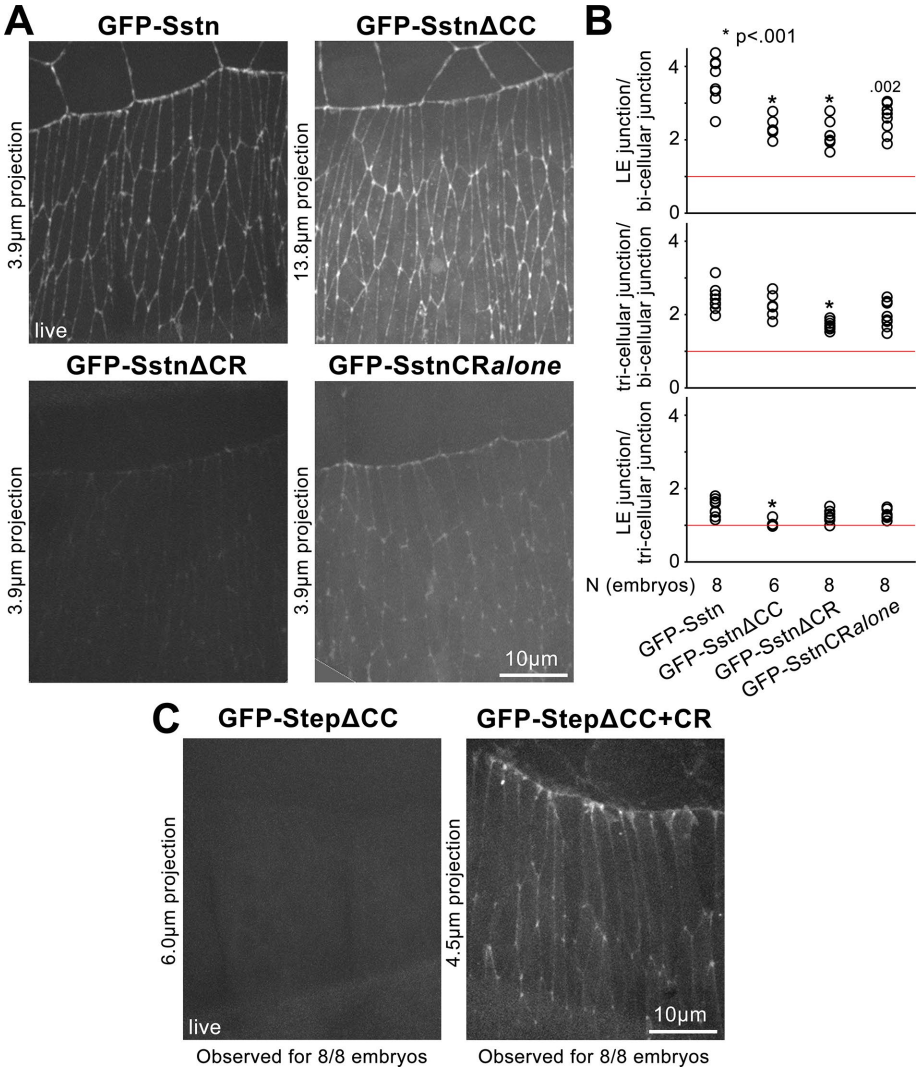

FIGURE 5: The Sstn CR is important for localization to LE and tricellular junctions. (A) Live imaging of embryos expressing full-length and domain deletion Sstn constructs in the lateral epidermis and amnioserosa (the top portion of each image) at dorsal closure. Constructs were expressed with *daughterless*-Gal4 and images were collected and adjusted with the same settings. Both GFP-Sstn and GFP-SstnΔCC showed strong junctional localization, with GFP-SstnΔCC showing less enrichment at LE junctions, whereas GFP-SstnΔCR displayed relatively weak junctional localization (observed for all embryos assessed—embryo numbers shown in B from two experiments). GFP-Sstn-CR was enriched at LE and tricellular junctions of the epidermis. (B) Signal intensity ratios between junctions of interest: "LE junction" refers to LE junctions of the epidermis; "tricellular junction" refers to tricellular junctions of epidermal cells to the rear; and "bicellular junction" refers to A–P bicellular junctions of epidermal cells to the rear. Asterisks indicate significant differences vs. full-length GFP-Sstn. Red lines indicate ratios of 1:1. Although GFP-SstnΔCC showed strong overall junctional localization, its signal ratios between the LE junctions and the other junction types were significantly reduced relative to the full-length construct. GFP-SstnΔCR signal ratios between the LE junctions and bicellular junctions, and between the tricellular junctions and the bicellular junctions, were both significantly reduced relative to the full-length construct. (C) Comparison of the weak, diffuse localization of GFP-StepΔCC with the strong junctional localization of GFP-StepΔCC+CR. Both constructs were imaged live with the same settings at dorsal closure in two experiments.

enrichment of endogenous Step-GFP and endogenous Sstn-GFP at epidermal LE and tricellular junctions (Figure 6B). The junctional Sstn-GFP signal was consistently lower than that of Step-GFP, and by quantifying LE junction signal intensities, we detected Sstn-GFP at 53, 75, and 80% of the local level of Step-GFP in comparisons of four to six embryos in each of three replicates (Figure 6B). Fixing and staining for DE-cad showed that both endogenously expressed proteins localized at the same apicolateral position as AJs with enrichment to epidermal LE and tricellular junctions (Figure 6C). Thus, endogenous Step and Sstn appear to colocalize at myosin-rich AJs, and junctional levels of Sstn seem to be somewhat lower than those of Step.

Junctional Step requires Sstn, and junctional Sstn depends substantially on Step

With cooverexpression Step and Sstn can increase each other's accumulation at myosin-rich cortical domains of the syncytial *Drosophila* embryo (Liu *et al.*, 2015). Moreover, depletion of Sstn reduces the localization of overexpressed Step to AJs of the *Drosophila* wing disc (Rauskolb *et al.*, 2019). To test how Sstn affects the localization of endogenous levels of Step, we probed GFP-tagged endogenous Step and antibody staining of endogenous Step in *sstn* mutants versus controls at dorsal closure. In control embryos, endogenous Step-GFP localized to epidermal LE and tricellular junctions, as discussed above (Figures 6B and 7A). Similarly, antibody staining for Step revealed clear enrichment at LE junctions, although other junctions were more difficult to discern (Figure 7B). For both Step probes, junctional localization was almost undetectable in *sstn* mutants (Figure 7, A and B). Live imaging could not detect Step-GFP expressed in the *sstn* mutants (unpublished data), but fixation revealed marginal Step-GFP enrichment along the LE (Figure 7A, arrows). Staining for DE-cad confirmed the localization of AJs and also showed an abnormally high frequency of multicellular rosettes in the *sstn* mutants (Figure 7, A and B; highlighted in yellow and quantified to the right). Thus, Sstn is required for recruiting Step to myosin-rich AJs, and *sstn* mutants display tissue distortions similar to those of *step* mutants (West *et al.*, 2017).

Next, we analyzed the localization of GFP-tagged endogenous Sstn expressed in *step* mutant or control embryos. Live imaging was able to detect the junctional localization of Sstn-GFP in both control and *step* mutant embryos, but the signal was substantially reduced in the *step* mutants (Figure 7C, arrows). Fixation and staining for DE-cad confirmed that junctional Sstn-GFP was substantially reduced in *step* mutants (Figure 7D). Together, these results show that the relationship between Sstn and Step is not simply linear, and that it is not equally reciprocal either. Sstn seems to have a greater effect on Step localization than Step does on Sstn localization.

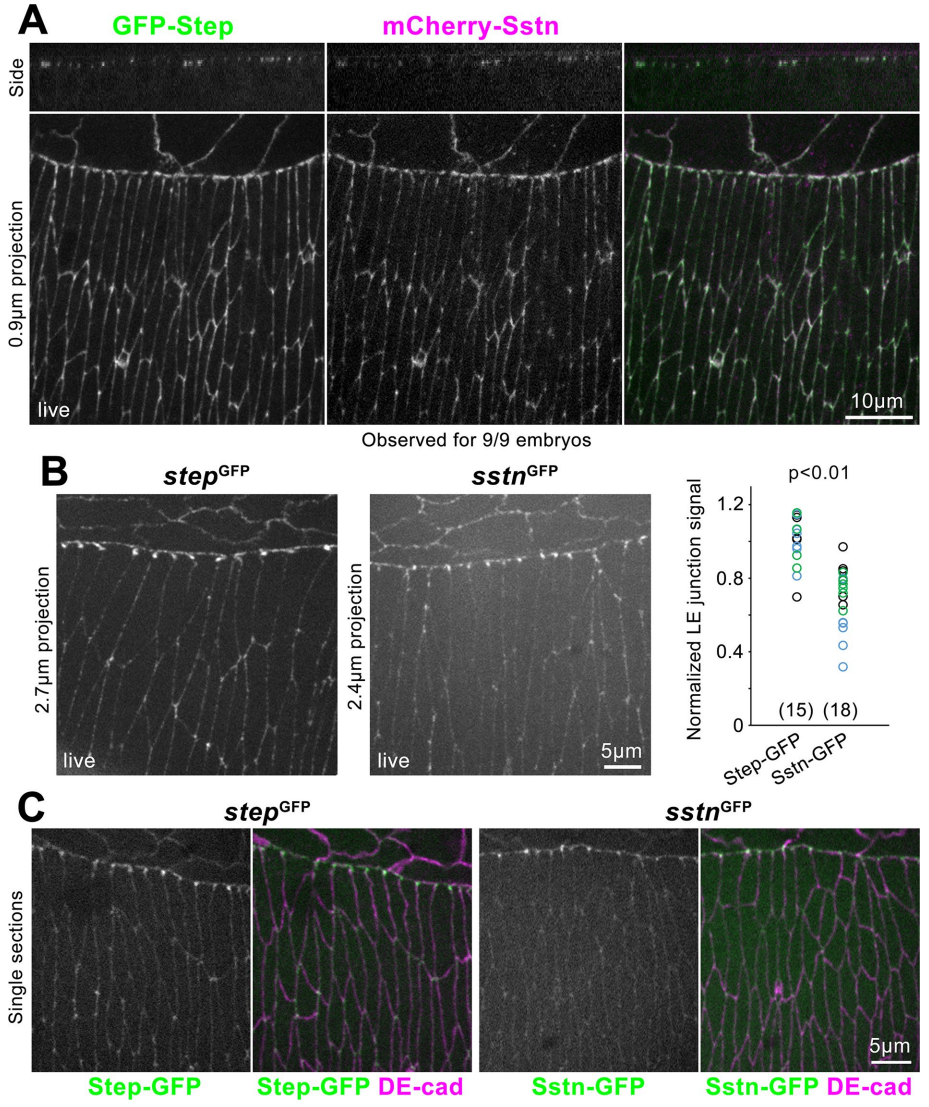

FIGURE 6: Step and Sstn colocalization at dorsal closure. (A) Side and surface views of GFP-Step and mCherry-Sstn expressed with *daughterless*-Gal4 in the same embryo and coimaged live. Both constructs localized to apicolateral epidermal junctions (side views) and showed strongest enrichment and colocalization to epidermal LE and tricellular junctions (surface views). (B) Surface views of Step-GFP and Sstn-GFP expressed from endogenous GFP insertion alleles and imaged live at dorsal closure with the same settings. The junctional distributions of the proteins were similar, but the junctional levels of Step-GFP were higher than those of Sstn-GFP. LE junction levels are quantified at right. Each replicate comparison is shown in a different color, and for each replicate the data were normalized to the average embryo values for the Step-GFP signal. Total embryo numbers are indicated in brackets. (C) Both Step-GFP and Sstn-GFP were enriched at epidermal LE junctions and tricellular junctions at the apicolateral position of DE-cad. Fixed and stained embryos shown.

The Step CC domain and the Step PH domain are each needed for proper tissue elongation

A *step* mutant rescue assay was previously used to show the requirement of Step Arf-GEF activity for proper epidermal organization during dorsal closure (West *et al.*, 2017). We used the same assay to test the roles of the Step CC and PH domains. With *paired*-Gal4, constructs were expressed in stripes in *step* mutant embryos, and multicellular rosette numbers were compared between construct-expressing and -nonexpressing tissue. Full-length Step-GFP substantially rescued the tissue distortions (Figure 8, top left). In contrast, expression of GFP-StepΔCC+CC[N*] failed to reduce the frequency of abnormal multicellular rosettes (Figure 8, bottom left). To test whether the CC domain's role in tissue organization was related to Sstn, we tested the ability of GFP-StepΔCC+CR to rescue the abnormal rosette numbers in *step* mutant tissue, and discovered that it had substantial rescue activity (Figure 8, bottom right). Thus, the CC domain of Step is needed for its function, and the CR of Sstn can substitute for this role.

GFP-StepΔPH also failed to reduce multicellular rosette numbers (Figure 8, top right). This lack of function was surprising because GFP-StepΔPH was effectively recruited to myosin-rich junctions of wild-type or *step* mutant embryos (Figures 1B and 2, A and B). Together, these data indicate that the PH domain is dispensable for the junctional localization of Step but is needed for Step to regulate epidermal organization. This relationship was observed previously for GEF-dead Step (West *et al.*, 2017), and thus it seems that both GEF activity and the PH domain have roles downstream from junctional recruitment.

DISCUSSION

Our data show that the CC domain of Step is a key determinant of its localization to myosin-rich AJs. This localization mechanism seems to depend on direct heterodimerization with the CC domain of Sstn, an interaction mediated by a hydrophobic face of the Step CC domain. For Sstn, a small region conserved across insects is critical for its localization to myosin-rich AJs, suggesting Sstn acts as an adaptor protein between Step and an unknown component of the junctions. Consistent with this model, Step and Sstn display strong colocalization at myosin-rich AJs. Moreover, Sstn is required for Step localization to these sites. However, the localization of Sstn also depends substantially on Step. Taken together, these data show how Sstn can act as an adaptor for recruiting Step to myosin-rich AJs, although the proteins also display partial codependence for localization to these sites. Downstream, the Sstn-Step interaction appears to aid the resolution of multicellular rosettes during dorsal closure.

Multiple results indicate that the junctional localization of Step relies on CC heterodimerization with Sstn. Blot overlay assays showed that the purified CC domains of each protein can interact directly, and allowed mapping of an interaction interface. Deletion of the Step CC domain, or mutation of its interaction interface with Sstn, eliminated junctional localization of overexpressed Step constructs in vivo. Highlighting that it is specifically Step-Sstn CC domain heterodimerization that is critical for the localization of Step to myosin-rich junctions, the Sstn CR was able

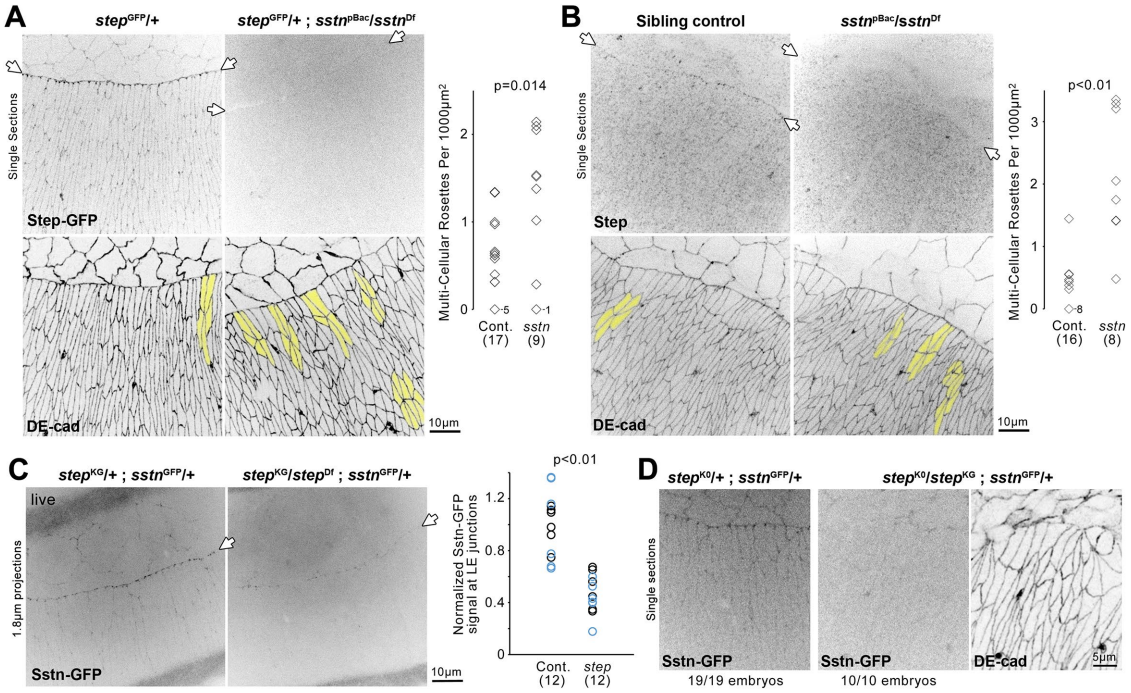

FIGURE 7: Step and Sstn promote each other's junctional localization. (A) *sstn* mutants were compared with control embryos both expressing the same dosage of *step*^{GFP}. The embryos were fixed and imaged at dorsal closure. A strong reduction of junctional Step-GFP was observed in the mutants, although a slight signal was detected along the epidermal LE (arrows). All images were taken at the same settings, and the observed pattern was consistent for comparisons of 9/9 mutant embryos and 17/17 control embryos from two experiments. DE-cad staining revealed AJ positioning and also showed distorted organization of the *sstn* mutant epidermis, including the abnormally frequent presence of multicellular rosettes (shaded in yellow and quantified to the right with embryo numbers in brackets). (B) Antibody staining of endogenous Step also revealed its loss from the epidermal LE (arrows) of *sstn* mutants vs. sibling controls in fixed dorsal closure embryos. All images were taken with the same settings, and the observed pattern was consistent for comparisons of 8/8 mutant embryos and 16/16 control embryos from two experiments. DE-cad staining revealed AJ positioning and also showed distorted organization of the *sstn* mutant epidermis (multicellular rosettes shaded in yellow and quantified to the right with embryo numbers in brackets). (C) Live imaging of Sstn-GFP revealed substantial loss from LE (arrows) and other junctions of the epidermis of *step* mutant embryos vs. sibling controls. LE junction levels are quantified at right. Two replicate comparisons are shown in different colors, and for each replicate the data were normalized to the average embryo values for the Sstn-GFP signal at LE junctions of the sibling controls. Embryo numbers are indicated in brackets. (D) Sstn-GFP was also observed to be lost from DE-cad–positive AJs of *step* mutants of a distinct genotype, in contrast to costained and comounted sibling controls.

to substitute for the Step CC domain to mediate Step localization and function. Finally, endogenous Step was lost from AJs of *sstn* mutants. Arguing against a role for Step CC homodimerization, replacement of the native CC domain with artificial CC domains optimized for parallel or antiparallel homodimerization failed to restore junctional localization. Arguing against a nonspecific effect of CC domain manipulations on Step protein stability, junctional localization was disrupted for four constructs each with a distinct CC domain manipulation, and a GFP-tagged construct of the CC domain alone was sufficient for localization to myosin-rich junctions. Thus, CC heterodimerization with Sstn seems critical for the junctional localization of Step.

We also found that a conserved region of Sstn mediates its localization to myosin-rich junctions. Similar to the CC domain of Step, the Sstn CR was necessary and sufficient for localization to such junctions, whereas the Sstn CC domain was relatively dispensable (except for full recruitment to LE junctions). What then is the localization mechanism of the CR? Presumably it binds a partner that is recruited by the junctional actomyosin network and/or opened for binding by actomyosin-based tension. It is important to note that the CR of Sstn is mainly conserved among insects (Liu *et al.*, 2015). Interestingly though, the closest mammalian homologue of Sstn, the protein FRMD4A, localizes to forming AJs and contains a CC domain that binds to the CC domain of cytohesin-1 (Ikenouchi and Umeda, 2010). In addition, FRMD4A contains an N-terminal FERM domain not found in Sstn and a direct binding site for Par-3 not conserved in Sstn (Ikenouchi and Umeda, 2010; Liu *et al.*, 2015). It is possible that one of these sites, or a separate site, in FRMD4A plays a role similar to the CR of Sstn. For example, Par-3 functions in the junctional recruitment of FRMD4A (Ikenouchi and Umeda, 2010). However, *Drosophila* Par-3 typically localizes to junctions depleted of actomyosin, as shown in the embryo germ band (Zallen and Wieschaus, 2004), for example.

Our discovery that the junctional localization of Sstn has partial dependence on Step indicates that their relationship is more complicated than the recruitment of an enzyme by a localized adaptor. This additional complexity may also explain the requirement of the Sstn CC domain for full recruitment of Sstn to LE junctions, and the substoichiometric junctional levels of Sstn relative to Step. We suggest two additional effects. First, Step and Sstn may both be more stable as Step-Sstn heterodimers than as individual proteins. Although isolated pieces of Step and Sstn

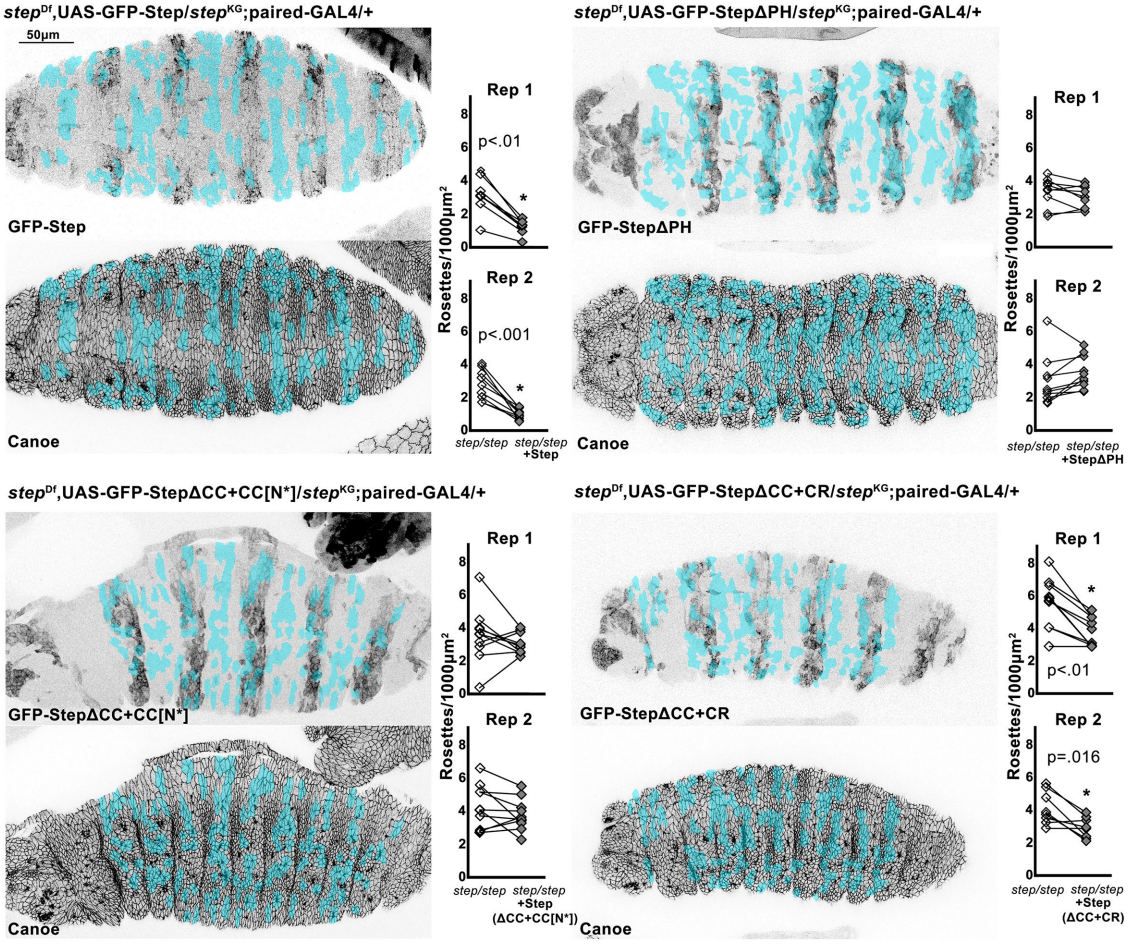

FIGURE 8: Abilities of Step constructs to rescue the tissue distortions of *step* mutant embryos. In a *step* mutant background, the indicated UAS constructs were expressed in epidermal stripes using *paired*-GAL4. The constructs and the AJ marker Canoe were imaged at dorsal closure, and quantifications of multicellular rosettes were compared between construct-expressing and –nonexpressing tissue. Example rosettes are labeled in cyan. Quantifications to the right of each pair of images are from two separate replicates, and rosette quantifications of construct-expressing and –nonexpressing tissue of the same embryo are connected with a line. Rescue of the abnormal rosettes was evident for expression of GFP-Step (top left) and of GFP-StepΔCC+CR (bottom right), but not for expression of GFP-StepΔCC+CC[N*] (bottom left) or of GFP-StepΔPH (top right).

(the Step CC and the Sstn CR) can localize to junctions when overexpressed, stabilized complexes might promote and/or maintain full junctional localization of Step and Sstn when expressed at endogenous levels. Endogenous Sstn would presumably provide adaptor function as part of such stabilized heterodimers. Second, additional proteins may contribute to Step localization. Indeed, it was recently reported that Ajuba, a tension-induced partner of junctional α-catenin (Yap *et al.*, 2018), 1) colocalizes with junctional Step and Sstn, 2) is required for recruitment of overexpressed Step to AJs, and 3) affects junctional myosin and tissue organization in ways very similar to Step and Sstn (Rauskolb *et al.*, 2019). Because no other portion of Step was sufficient for its AJ localization in the absence of its CC domain, interactions with additional proteins may involve the CC domain, an idea consistent with the ability of CC-mediated interactions to support trimers, tetramers, or even heptamers (Grigoryan and Keating, 2008). It is important to note that these two proposals are not mutually exclusive. During *Drosophila* embryo development, it is tempting to speculate that the first mechanism might dominate for actomyosin regulation in the syncytial embryo, when epithelial cells, and thus AJs, are absent. The second mechanism may then arise during gastrulation when actomyosin-associated AJs are subjected to tension.

Our study is significant for defining a molecular mechanism that recruits Step to myosin-rich junctions for an established role in regulating actomyosin activity at these sites (West *et al.*, 2017). Tension-based conformational change of α-catenin also recruits actin-binding proteins to reinforce junction–actomyosin connections (Leckband and de Rooij, 2014; Pinheiro and Bellaïche, 2018; Yap *et al.*, 2018). These mechanisms may work together to modify both the generation of junctional tension and resistance to it.

MATERIALS AND METHODS

Previously established *Drosophila* lines

The following alleles were used: $sstn^{Df(Df(3L)BSC441)}$ (Bloomington *Drosophila* Stock Center [BDSC] #24945); $sstn^{c04515}$ (Exelixis; Stock #c04515); $step^{Df(Df(2L)BSC150)}$ (BDSC; #9509); $step^{KG09493}$ and $step^{K08110}$ (gifts from M. Hoch, Life and Medical Science Institute of Bonn, Germany); zip^{GFP} (FlyTrap; Stock #CC01626; BDSC; #51564).

The following UAS constructs were used: UAS-GFP at attp2 (gift of U. Tepass, University of Toronto, Canada); UAS-GFP-Sstn at attp40 (Liu *et al.*, 2015); UAS-GFP-SstnΔCC at attp40 (Liu *et al.*, 2015); UAS-GFP-SstnΔCR at attp40 (Liu *et al.*, 2015); UAS-mCherry-Sstn at attp2 (Liu *et al.*, 2015); UAS-GFP-Step (RNA interference [RNAi]-resistant) at attp40 (Lee and Harris, 2013); UAS-GFP-StepΔCC at attp40 (Liu *et al.*, 2015); UAS-GFP-StepΔPH (RNAi-resistant) at attp40 (Lee *et al.*, 2015).

UAS constructs were driven using either *daughterless*-Gal4 (gift of U. Tepass) or *paired*-Gal4 (BDSC; #1947).

The following construct was also used: tGPH (BDSC #8163). It was described as GFP-StepPH+PB*alone*.

Generated UAS constructs

For StepCC*alone*-GFP, the Step CC domain (amino acids [aa] 25–70) was PCR amplified from the *step* isoform A cDNA (RE34385; Canadian *Drosophila* Microarray Centre) using 5′-CCGGAACCAATTCAGTCGACATGCCAGAACTTACACCGG-3′ (forward) and 5′-AAGCTGGGTCTAGATATCTCGAGTGGGGCACATCCAGC-3′ (reverse) primers (all primers from Life Technologies), and cloned into the pENTR vector using *Sal*I and *Xho*I restriction sites. Gateway cloning (Life Technologies) recombined the construct into pPWG downstream from a UASp promoter for C-terminal enhanced GFP tagging. An attB recombination site cloned into the pPWG Nsi1 site targeted the vector to the attp40 recombination site on chromosome 2 (BestGene).

For GFP-SstnCR*alone*, the Sstn CR (aa 576–635) was PCR amplified from the *sstn* cDNA (RE36140; *Drosophila* Genomics Resource Center) using 5′-CAGTCGACTGGATCCCCCAGTAACAGTGGCCAC-3′ (forward) and 5′-GGGTCTAGATATCTCGAGTCAATTAGGATTTCCGCCC-3′ (reverse) primers, and cloned into the pENTR vector using *Bam*HI and *Xho*I restriction sites. GFP tagging was the same as above except the pPGW vector was used and the construct was targeted to the attp2 recombination site (BestGene).

To replace the CC domain of Step with other protein sequences, we used *Sal*I and *Bsa*I restriction sites that flank either side of the sequence encoding the CC domain to excise this portion of the *step* cDNA within the pENTR vector. Synthetic DNA constructs were generated (GenScript) that spanned the *step* sequence between the restriction sites but replaced the sequence encoding the CC domain of Step (Figure 3B) with sequences encoding alternate peptides (maintaining the flanking proline residues shown for the Step CC in Figure 3B). After restriction enzyme digestion, the synthetic constructs were ligated into the excised *step* construct, and then the hybrid construct was recombined into pPGW. These final constructs were each targeted to the attp40 recombination site in transgenic flies (BestGene). For GFP-StepΔCC+CC[N*], the Step CC was altered to change its first seven leucines and isoleucines to serine residues (as in Figure 3B). For GFP-StepΔCC+APH, the sequence encoded the APH synthetic CC domain (MKQLEKELKQLEKELQAIEKQLAQLQWKAQARKKKLAQLKKKLQA with a 3′ proline as a linker; Gurnon *et al.*, 2003). For GFP-StepΔCC+E/K42, the sequence encoded VSSLESK repeated six times (Graddis *et al.*, 1993). For GFP-StepΔCC+CR, the sequence encoded the Sstn CR (aa 576–635).

Generated GFP-tagged *sstn* allele

The CRISPR-Cas9 tagging of Sstn with GFP was based on an existing protocol (Harris *et al.*, 2016).

The donor construct was generated in two steps. For the first construction step, the NEBuilder HIFI DNA Assembly Cloning Kit (New England Biolabs) connected three pieces: 1) a Phusion high-fidelity DNA polymerase (New England Biolabs) PCR amplicon of a portion of the *sstn* genomic DNA Bac clone (BACPAC resources center; #BACR18G16) covering sequence 5′ of the stop codon and replacing the stop codon with a short sequence overlapping with the 5′ of the GFP sequence (forward primer, 5′-CGCGGACATATGCACACCTGCTAATATCAGCTACG-3′; reverse primer, 5′-CCTTGCTCACCATATTAGGATTTCCGCCCTCCTT-3′); 2) a Phusion high-fidelity DNA polymerase PCR amplicon of the sequence of GFP plus overlapping ends with the *sstn* sequence and the pDSRed vector sequence (forward primer, 5′-GAGGGCGGAAATCCTAATATGGTGAGCAAGGGC-3′; reverse primer, 5′-AGTTGGGGCACTACGATCTCACTTGTAC-3′; template, PPWG vector); and 3) the pDSRed vector (gift of K. O'Connor Giles, University of Wisconsin; forward primer CATGGACGAGCTGTACAAGTGAGATCGTAGTGCCC; reverse primer 5′-TTAGCAGGTGTGCATATGTCCGCGGCCG-3′).

For the second construction step, a 1 kb sequence of *sstn* 3′ to the stop codon was synthesized (GenScript) based on the *sstn* genomic DNA Bac clone (BACR18G16) with restriction enzyme sites of *Bgl*II and *Xho*I added at the ends. This synthesized DNA was ligated with the first assembled construct, which was cut with *Bgl*II and *Xho*I.

The g-RNA sequence was selected with an online tool (http://tools.flycrispr.molbio.wisc.edu/targetFinder/) and contained a PAM site close to the *sstn* stop codon (g-RNA sequence, 5′-GGCCACTTTCCAGCCGTACA-3′). To generate the g-RNA construct, the g-RNA sequence was ligated into the pCDf3 vector (gift of K. O'Connor Giles). The corresponding PAM site in the donor construct was mutated from 5′-GGCCACTTTCCAGCCGTACAAGGAAGTGACGAAACCC-3′ to 5′-GGCCACTTTCCAGCCGTACAATCAAGTGACGAAACCC-3′. The complete donor construct was sequenced for confirmation.

Both the g-RNA and the donor construct were injected into yw;;nos-Cas9 III-attp2 flies. The injection and subsequent screening, Cas9 removal, and genetic balancing were done by Bestgene (Plan RI). Viable and fertile homozygous flies were utilized for the study with the insertion confirmed by PCR and sequencing.

Generated GFP-tagged *step* allele

The CRISPR-Cas9 tagging of Step with GFP was based on an existing protocol (Harris *et al.*, 2016).

The NEBuilder HIFI DNA Assembly Cloning Kit (New England Biolabs) was used to generate the donor construct in two steps. The first step included three pieces: 1) 1 kb upstream of the *step* stop codon was amplified (forward primer, 5′-GCGGACATATGCACACCTGCACACATGCTATGT-3′; reverse primer, 5′-CCCTTGCTCACCATACTCTTGCTGAGTGCCTTT-3′) with the template of *step* genomic DNA (BACR09H20, BACPAC resources center); 2) the GFP sequence with a new stop codon incorporated (forward primer, 5′-GGCACTCAGCAAGAGTATGGTGAGCAAGGGC-3′; reverse primer, 5′-GGGCACTACGATCTCACTTGTACAGCTCGTCCAT-3′) with the template of the PPWG vector; and 3) the pDSRed vector (gift of K. O'Connor Giles, University of Wisconsin; forward primer CATGGACGAGCTGTACAAGTGAGATCGTAGTGCCC, reverse primer 5′-GCATGTGTGCAGGTGTGCATATGTCCGC-3′).

The second step for assembling the donor construct amplified 1 kb downstream of the *step* stop codon (forward primer, 5′-GCCTAGGCCTTCTGCAGTACTAACAAGCAGC-3′; reverse primer, 5′-AGCCTCGAGCGGGCAATTTATACATTCTT-3′; from the *step* genomic DNA). This downstream sequence was then assembled into the vector from the first step (forward primer 5′-GTATAAATTGCCCGCTCGAGGCTCTTC-3′, reverse primer 5′- GCTTGTTAGTACTGCAGAAGGCCTAGGC-3′).

The g-RNA was found using an online tool (http://tools.flycrispr.molbio.wisc.edu/targetFinder/) with a PAM site near the *step* stop codon (g-RNA sequence: 5′-CGGAGGAAGATCAGCAGGAG-3′). To generate the g-RNA, the sequence was ligated into the *Bbs*1 site of the pCDf3 vector (gift of K. O'Connor Giles, University of Wisconsin). The corresponding PAM site in the donor construct was mutated from 5′-GCATGTCCGCTGTTACGGAGGAAGATCAGC-3′ to 5′-GCTGATCTTCCTCCGTAACAGCGGACATGC-3′. The complete donor construct was sequenced for confirmation.

Both the g-RNA and the donor construct were injected into yw;;nos-Cas9 III-attp2 flies. The injection and subsequent screening, Cas9 removal, and genetic balancing were done by Bestgene (Plan RI). Viable and fertile homozygous flies were utilized for the study with the insertion confirmed by PCR and sequencing.

Synthesized lines

For complex genotypes with alleles on separate chromosomes, standard *Drosophila* genetics was used for synthesis. For the recombinant chromosomes of $step^{Df(Df(2L)BSC150)}$ with UAS constructs, PCR was used to confirm the presence of $step^{Df(Df(2L)BSC150)}$ by amplifying the opposite flanking regions of the deletion, and the UAS constructs were detected using a linked miniwhite cassette.

Antibody staining of embryos

Embryos were collected from apple juice agar plates (25 g agar; 250 ml store-bought apple juice; 12.5 g store-bought granulated white sugar; 10 ml, 10% Tegosept [in ethanol]) using a brush into 0.1% Triton X-100, and washed three times. Dechorionation was performed with 50% bleach for 4 min, and the embryos were then washed another three times with 0.1% Triton X-100. Fixation was performed using 1:1 3.7% formaldehyde in phosphate-buffered saline (PBS):heptane for 20 min. Embryos were devitellinized by shaking in methanol and rinsed three times afterward with methanol. Blocking and staining were conducted with PBS with 1% goat serum, 1% sodium azide, and 0.1% Triton X-100. Primary antibodies were guinea pig anti-Step (1:350; gift of M. Hoch), rabbit anti-Canoe (1:1000; gift of M. Peifer, University of North Carolina, Chapel Hill), and rat anti–DE-cadherin (1:100; Developmental Studies Hybridoma Bank). Secondary antibodies were conjugated to Alexa Fluor 546 and 647 (Life Technologies). Mounting of fixed and immunostained embryos was with Aqua Polymount (Polysciences).

Live imaging preparation

Embryos for live imaging were collected from apple juice agar plates using a brush into 0.1% Triton X-100, and washed three times. Dechorionation was performed with 50% bleach for 4 min, and the embryos were then washed another three times with 0.1% Triton X-100. Embryos were then mounted on a glass coverslip using tape glue dissolved in heptane and overlaid with halocarbon oil (series 700; Halocarbon Products). The coverslip, with the embryos facing up, was set into the bottom of a glass-bottom culture dish with its original coverslip removed.

Embryo imaging

Most imaging was done using a spinning disk confocal microscope (Quorum Technologies) with a Hamamatsu EM CCD camera. Image capture was performed using Volocity software (PerkinElmer). The imaging took place at room temperature at 63× magnification (Plan-Apochromat; NA 1.4). Samples were mounted on a piezo stage and z-stacks were imaged with 0.3 µm spacing.

Whole embryo imaging of Figure 8 was performed with a Leica TCS SP8 confocal system at RT with a 40× NA 1.4 objective (Leica), and 300 nm step sizes.

Image quantification and manipulation

For local protein levels within each embryo, there were three junctions of interest: 1) LE junctions, 2) tricellular junctions within the lateral epidermal sheet, and 3) A–P bicellular junctions within the lateral epidermal sheet. Any cell at least one cell away from the LE cells was considered part of the lateral epidermis. Per embryo, each junction type was measured from five separate cells showing the highest signal intensity. For each measurement, a small circle with was drawn over the center of the junction of interest and the mean fluorescence was acquired using Fiji (Schindelin *et al.*, 2012). To correct the measurement for background, signal in the cytoplasm of the cell was also measured using the same method and the mean fluorescence was subtracted from the junction measurement. Means of the five background-corrected measurements of each junction type were calculated for each embryo, resulting in one value per junction type per embryo. These single junction values were then compared to calculate junction:junction ratios within each embryo.

For epithelial rosette identification and quantification, the methodology from West *et al.* (2017) was used. Rosette structures were considered as five or more cells with a common vertex within a square area of 1.6 μm^2.

Statistical significance for pairwise comparisons was calculated using Student's *t* tests in Excel (Microsoft).

Blot overlays

For glutathione S-transferase (GST)–StepCC, the Step CC domain was PCR amplified using 5′-CCCCTGGGATCCCCGGAGCAGCAAAAAC-3′ (forward) and 5′-ATGCGGCCGCTCGAGTTAGGGCACATCCAG-3′ (reverse) primers, and cloned into the pGEX-6p2 vector using *Bam*HI and *Xho*I restriction sites. For GST-SstnCC, the Sstn CC domain (aa 60–87) was PCR amplified using 5′-GGCCCCTGGGATCCCCAAAGGTTAGGAAG-3′ (forward) and 5′-GGCCGCTCGAGTTAGGGTTGGTAATTG-3′ (reverse) primers, and cloned into the pGEX-6p2 vector using *Bam*HI and *Xho*I restriction sites.

For maltose-binding protein (MBP)–StepCC, the Step CC domain was PCR amplified using 5′-CAGAATTCGGATCCCCGGAGCAGCAAAAAC-3′ (forward) and 5′-CAGTGCCAAGCTTAGGGCACATCC-3′ (reverse) primers, and cloned into the pMal-C2X vector using *Bam*HI and *Hin*dIII restriction sites. For MBP-SstnCC, the Sstn CC domain was PCR amplified using 5′-CAGAATTCGGATCCCCAAAGGTTAGGAAGGAG-3′ (forward) and 5′-CGGCCAGTGCCAAGCTTAGGGTTGGTAATTGTC-3′ (reverse) primers, and cloned into the pMal-C2X vector using *Bam*HI and *Hin*dIII restriction sites.

For MBP-tagged Step mutant CC domains, the specific mutant fragments were synthesized (GenScript) and inserted into pMalC2X with *Bam*HI N-terminal sites and *Hin*dIII C-terminal sites.

Using the supplier's instructions, the MBP and GST fusion protein constructs were inoculated in BL21 competent cells and induced using 0.1 mM isopropyl-β-D-thiogalactoside (IPTG) (final concentration). The cells were pelleted at 3500 × *g* and 4°C and lysed with 20 ml PBS-T (PBS with 1% Triton X-100) with 2 µg/ml aprotinin, 1 µg/ml leupeptin, 25 µg/ml phenylmethylsulfonyl fluoride, and 1 mg/ml lysozyme. The mixture was incubated at room temperature for 40 min and centrifuged at 12,000 × *g* for 20 min at 4°C. The supernatant was run through the purification column with either Pierce glutathione agarose (Thermo Scientific) for GST fusion

proteins or amylose resin (New England Biolabs) for MBP fusion proteins. Following washes, the proteins were eluted with either GST elution buffer (10 mM glutathione, 50 mM Tris-HCl, pH 9.0, and 15% glycerol) or MBP elution buffer (10 mM maltose, 200 mM NaCl, 20 mM Tris-HCl, 1 mM EDTA, 1 mM dithiothreitol [DTT], pH 7.4).

Purified GST and MBP fusion proteins were first individually tested using GST and MBP antibodies (New England Biolabs) on diagnostic Western blots. For blot overlays, MBP fusion proteins (1–3 µg) were separated with 10% SDS–PAGE and individually blotted on nitrocellulose. Blocking was done with 5% milk in TBST buffer (8.0 g of NaCl, 2.42 g of Tris, and 1 ml of Tween-20 in 1 l of double-distilled H_2O, pH adjusted to 8.0). Blots were incubated with each GST fusion protein (~7 µg) in TBST buffer and 5% milk, washed, incubated with GST antibodies (raised in rabbit–lab generated) in TBST buffer and 5% milk, washed, incubated with horseradish peroxidase–conjugated goat anti-rabbit antibodies, washed, and incubated with chemiluminescent reagents (Thermo Fisher Scientific). Imaging of the blots was done on a ChemiDoc XRS (Bio-Rad). For each binding assay, control and noninteracting proteins were adjusted so they were present at higher molar levels than interacting proteins (levels were evaluated based on diagnostic Western blots).

Protein structure prediction and visualization

The Step CC structure was predicted with the Phyre2 server (Kelley *et al.*, 2015). After conversion to .c3d file format with the National Center for Biotechnology Vast Search Tool (Madej *et al.*, 2014), the file was analyzed with the CN3D viewer to identify hydrophobic residues in the 3D structure (Wang *et al.*, 2000).

ACKNOWLEDGMENTS

We are thankful for reagents from M. Hoch, K. O'Connor Giles, M. Peifer, U. Tepass, the Bloomington *Drosophila* Stock Center, the Canadian *Drosophila* Microarray Centre, the *Drosophila* Genomics Resource Center, the BACPAC resources center, and the Developmental Studies Hybridoma Bank. We thank E. Hunt for commenting on the manuscript. This work was supported by a Canadian Institutes of Health Research operating grant (Grant no. 82829) to T. H. J.W. was supported by an Ontario Graduate Scholarship.

REFERENCES

Britton JS, Lockwood WK, Li L, Cohen SM, Edgar BA (2002). *Drosophila*'s insulin/PI3-kinase pathway coordinates cellular metabolism with nutritional conditions. Dev Cell 2, 239–249.

Cadwell CM, Su W, Kowalczyk AP (2016). Cadherin tales: regulation of cadherin function by endocytic membrane trafficking. Traffic 17, 1262–1271.

Campinho P, Behrndt M, Ranft J, Risler T, Minc N, Heisenberg CP (2013). Tension-oriented cell divisions limit anisotropic tissue tension in epithelial spreading during zebrafish epiboly. Nat Cell Biol 15, 1405–1414.

Cohen LA, Honda A, Varnai P, Brown FD, Balla T, Donaldson JG (2007). Active Arf6 recruits ARNO/cytohesin GEFs to the PM by binding their PH domains. Mol Biol Cell 18, 2244–2253.

DiNitto JP, Delprato A, Gabe Lee MT, Cronin TC, Huang S, Guilherme A, Czech MP, Lambright DG (2007). Structural basis and mechanism of autoregulation in 3-phosphoinositide-dependent Grp1 family Arf GTPase exchange factors. Mol Cell 28, 569–583.

Donaldson JG, Jackson CL (2011). ARF family G proteins and their regulators: roles in membrane transport, development and disease. Nat Rev Mol Cell Biol 12, 362–375.

Gillingham AK, Munro S (2007). The small G proteins of the Arf family and their regulators. Annu Rev Cell Dev Biol 23, 579–611.

Graddis TJ, Myszka DG, Chaiken IM (1993). Controlled formation of model homo- and heterodimer coiled coil polypeptides. Biochemistry 32, 12664–12671.

Grigoryan G, Keating AE (2008). Structural specificity in coiled-coil interactions. Curr Opin Struct Biol 18, 477–483.

Gurnon DG, Whitaker JA, Oakley MG (2003). Design and characterization of a homodimeric antiparallel coiled coil. J Am Chem Soc 125, 7518–7519.

Hahn I, Fuss B, Peters A, Werner T, Sieberg A, Gosejacob D, Hoch M (2013). The *Drosophila* Arf GEF Steppke controls MAPK activation in EGFR signaling. J Cell Sci 126, 2470–2479.

Harris TJ, Tepass U (2010). Adherens junctions: from molecules to morphogenesis. Nat Rev Mol Cell Biol 11, 502–514.

Harris KP, Zhang YV, Piccioli ZD, Perrimon N, Littleton JT (2016). The postsynaptic t-SNARE Syntaxin 4 controls traffic of Neuroligin 1 and Synaptotagmin 4 to regulate retrograde signaling. Elife 5, e13881.

Hiester KG, Santy LC (2013). The cytohesin coiled-coil domain interacts with threonine 276 to control membrane association. PLoS One 8, e82084.

Hofmann I, Thompson A, Sanderson CM, Munro S (2007). The Arl4 family of small G proteins can recruit the cytohesin Arf6 exchange factors to the plasma membrane. Curr Biol 17, 711–716.

Ikenouchi J, Umeda M (2010). FRMD4A regulates epithelial polarity by connecting Arf6 activation with the PAR complex. Proc Natl Acad Sci USA 107, 748–753.

Kelley LA, Mezulis S, Yates CM, Wass MN, Sternberg MJ (2015). The Phyre2 web portal for protein modeling, prediction and analysis. Nat Protoc 10, 845–858.

Kiehart DP, Crawford JM, Aristotelous A, Venakides S, Edwards GS (2017). Cell sheet morphogenesis: dorsal closure in *Drosophilamelanogaster* as a model system. Annu Rev Cell Dev Biol 33, 169–202.

Klarlund JK, Tsiaras W, Holik JJ, Chawla A, Czech MP (2000). Distinct polyphosphoinositide binding selectivities for pleckstrin homology domains of GRP1-like proteins based on diglycine versus triglycine motifs. J Biol Chem 275, 32816–32821.

Leckband DE, de Rooij J (2014). Cadherin adhesion and mechanotransduction. Annu Rev Cell Dev Biol 30, 291–315.

Lee DM, Harris TJ (2013). An Arf-GEF regulates antagonism between endocytosis and the cytoskeleton for *Drosophila* blastoderm development. Curr Biol 23, 2110–2120.

Lee DM, Rodrigues FF, Yu CG, Swan M, Harris TJ (2015). PH domain-Arf G protein interactions localize the Arf-GEF Steppke for cleavage furrow regulation in *Drosophila*. PLoS One 10, e0142562.

Li J, Malaby AW, Famulok M, Sabe H, Lambright DG, Hsu VW (2012). Grp1 plays a key role in linking insulin signaling to glut4 recycling. Dev Cell 22, 1286–1298.

Lim J, Zhou M, Veenstra TD, Morrison DK (2010). The CNK1 scaffold binds cytohesins and promotes insulin pathway signaling. Genes Dev 24, 1496–1506.

Liu J, Lee DM, Yu CG, Angers S, Harris TJ (2015). Stepping stone: a cytohesin adaptor for membrane cytoskeleton restraint in the syncytial *Drosophila* embryo. Mol Biol Cell 26, 711–725.

Madej T, Lanczycki CJ, Zhang D, Thiessen PA, Geer RC, Marchler-Bauer A, Bryant SH (2014). MMDB and VAST+: tracking structural similarities between macromolecular complexes. Nucleic Acids Res 42, D297–D303.

Major RJ, Irvine KD (2006). Localization and requirement for Myosin II at the dorsal-ventral compartment boundary of the *Drosophila* wing. Dev Dyn 235, 3051–3058.

Manning LA, Perez-Vale KZ, Schaefer KN, Sewell MT, Peifer M (2019). The *Drosophila* Afadin and ZO-1 homologues Canoe and Polychaetoid act in parallel to maintain epithelial integrity when challenged by adherens junction remodeling. Mol Biol Cell 30, 1879–2095.

Mason JM, Arndt KM (2004). Coiled coil domains: stability, specificity, and biological implications. Chembiochem 5, 170–176.

Nevrivy DJ, Peterson VJ, Avram D, Ishmael JE, Hansen SG, Dowell P, Hruby DE, Dawson MI, Leid M (2000). Interaction of GRASP, a protein encoded by a novel retinoic acid-induced gene, with members of the cytohesin family of guanine nucleotide exchange factors. J Biol Chem 275, 16827–16836.

Pinheiro D, Bellaïche Y (2018). Mechanical force-driven adherens junction remodeling and epithelial dynamics. Dev Cell 47, 3–19.

Rafiq NB, Lieu ZZ, Jiang T, Yu CH, Matsudaira P, Jones GE, Bershadsky AD (2017). Podosome assembly is controlled by the GTPase ARF1 and its nucleotide exchange factor ARNO. J Cell Biol 216, 181–197.

Ratheesh A, Priya R, Yap AS (2013). Coordinating Rho and Rac: the regulation of Rho GTPase signaling and cadherin junctions. Prog Mol Biol Transl Sci 116, 49–68.

Rauskolb C, Cervantes E, Madere F, Irvine KD (2019). Organization and function of tension-dependent complexes at adherens junctions. J Cell Sci 132, jcs224063.
Reyes CC, Jin M, Breznau EB, Espino R, Delgado-Gonzalo R, Goryachev AB, Miller AL (2014). Anillin regulates cell-cell junction integrity by organizing junctional accumulation of Rho-GTP and actomyosin. Curr Biol 24, 1263–1270.
Schindelin J, Arganda-Carreras I, Frise E, Kaynig V, Longair M, Pietzsch T, Preibisch S, Rueden C, Saalfeld S, Schmid B, *et al.* (2012). Fiji: an open-source platform for biological-image analysis. Nat Methods 9, 676–682.
Takeichi M (2014). Dynamic contacts: rearranging adherens junctions to drive epithelial remodelling. Nat Rev Mol Cell Biol 15, 397–410.
Wang Y, Geer LY, Chappey C, Kans JA, Bryant SH (2000). Cn3D: sequence and structure views for Entrez. Trends Biochem Sci 25, 300–302.
West JJ, Zulueta-Coarasa T, Maier JA, Lee DM, Bruce AEE, Fernandez-Gonzalez R, Harris TJC (2017). An actomyosin-Arf-GEF negative feedback loop for tissue elongation under stress. Curr Biol 27, 2260–2270.e2265.
Yap AS, Duszyc K, Viasnoff V (2018). Mechanosensing and mechanotransduction at cell-cell junctions. Cold Spring Harb Perspect Biol 10, a028761.
Young PE, Richman AM, Ketchum AS, Kiehart DP (1993). Morphogenesis in *Drosophila* requires nonmuscle myosin heavy chain function. Genes Dev 7, 29–41.
Zallen JA, Wieschaus E (2004). Patterned gene expression directs bipolar planar polarity in *Drosophila*. Dev Cell 6, 343–355.